Polymer 49 (2008) 2669–2677

Contents lists available at ScienceDirect

Polymer

journal homepage: www.elsevier.com/locate/polymer

SAXS study of the lamellar–cylindrical transition in the PI-*b*-P2VP(OG) supramolecules' system

Sasa Bondzic [a], Evgeny Polushkin [a], Janne Ruokolainen [b], Gerrit ten Brinke [a,*]

[a] Laboratory of Polymer Chemistry, Zernike Institute for Advanced Materials, University of Groningen, Nijenborgh 4, 9747 AG Groningen, The Netherlands
[b] Department of Engineering Physics and Mathematics and Center for New Materials, Helsinki University of Technology, P.O. box 2200, FIN-02015 HUT Espoo, Finland

ARTICLE INFO

Article history:
Received 20 December 2007
Received in revised form 31 March 2008
Accepted 1 April 2008
Available online 11 April 2008

Keywords:
Self-assembly
Supramolecules
Order–order transitions

ABSTRACT

A detailed SAXS study of self-assembled block copolymer-based supramolecules composed of a polyisoprene-*block*-poly(2-vinylpyridine) diblock copolymer and octyl gallate that is hydrogen bonded to the vinylpyridine block in a stoichiometric ratio is presented. The changes in the system morphology with temperature are investigated both at rest and under oscillatory shear. In between the lamellar-to-cylindrical transition a new intermediate structure, identified as a deformed hexagonal structure (DHS), was observed. Being at rest the DHS is argued to consist of ellipsoidal cylinders that adopt a more regular circular shape when the sample is subjected to shear. These results are discussed in terms of hydrogen bond breaking under shear.

1. Introduction

During the last decades self-assembly of block copolymers continues to be one of the most challenging topics in polymer science [1–10]. For a variety of block copolymer systems a large number of different self-assembled nanostructures have been observed. For diblock copolymers the well-known examples are the classical body-centered-cubic, the hexagonally packed cylindrical (CYL) and the lamellar (LAM) morphology as well as the more complex gyroid structure. Depending on the experimental conditions, a desired morphology can be easily tailored, and this possibility itself is of great interest for applications in such areas as functional materials and nanotechnology. In particular, the use of ordered block copolymer systems to produce nanotemplates has attracted considerable attention lately. Among various ways to produce such templates, the supramolecular approach involving the preparation of comb-shaped diblock copolymer-based molecules by means of hydrogen bonding between amphiphilic molecules and diblock copolymers stands out as a very attractive route. Originally block copolymer-based comb-shaped supramolecules were used to produce materials with a hierarchical structure-in-structure morphology. The most frequently investigated systems were based on PS-*b*-P4VP diblock copolymers, consisting of a polystyrene (PS) and a poly(4-vinylpyridine) (P4VP) block. The latter can be either directly hydrogen bonded with 3-pentadecylphenol (PDP) to form a non-charged PS-*b*-P4VP(PDP)$_x$ complex, or first protonated with methanesulfonic acid (MSA) and then hydrogen bonded with PDP, resulting thus in a charged PS-*b*-P4VP(MSA)$_y$(PDP)$_x$ complex. Here x and y denote the ratio between the number of the pyridine groups and the molecules of PDP and MSA, respectively [11–14]. As for template applications, the clear advantage of such supramolecular systems is the fact that after formation of the ordered morphology the amphiphilic molecules may be simply removed by dissolving them in a selective solvent. The potential of this approach has already been amply demonstrated by the preparation of nanoporous membranes [12–18] and core-shell nano-rods [19–21].

Besides the PS-*b*-P4VP(PDP)$_x$ system, another potentially interesting system to create nano-porous membranes is the hydrogen bonded complex of polyisoprene-*block*-poly(2-vinylpyridine) (PI-*b*-P2VP) and octyl gallate (OG). For this particular diblock copolymer PDP is not a suitable compound since its high solubility in PI gives rise to a large uncertainty in the supramolecular system composition. In contrast to P4VP(PDP), P2VP(OG) domains do not microphase separate and, therefore, no hierarchically ordered structures are observed in the case of the PI-*b*-P2VP(OG) systems. However, the presence of an additional short length scale structure is not essential for most of the template applications. Microphase separation on a large length scale, i.e., between the PI coil block and the P2VP(OG) comb block, does readily occur. Depending on the amount of OG in the PI-*b*-P2VP(OG)$_x$ the system shows a very rich phase behavior [22]. One specific aspect of it, namely the complex pathway from LAM to CYL structure on heating is the subject of this study.

* Corresponding author. Tel.: +31 050 363 4509; fax: +31 050 363 4400.
E-mail address: g.ten.brinke@rug.nl (G. ten Brinke).

0032-3861/$ – see front matter © 2008 Elsevier Ltd. All rights reserved.
doi:10.1016/j.polymer.2008.04.011

For classical diblock copolymer systems thermoreversible order–order transitions (OOT), in particular cylindrical-to-spherical [23–26] and cylindrical-to-gyroid transitions [27–29], have been reported and extensively discussed in the literature. Also considerable attention has been paid to the mechanism of the transformation of lamellae to cylinders and some physical models to describe this process have already been put forward. Hamley et al. [30] have reported on two model mesostructures, hexagonally modulated (HML) and hexagonally perforated lamellae (HPL) that could occur as intermediates between LAM and CYL phases during this OOT. The existence of a HPL structure, as well as a tetragonally perforated layers (TPL) structure, was also proposed by Ryu et al. [31]. Hajduk et al. [32] and Jeong et al. [33] reported on a modified layer (ML) structure consisting of parallel cylinders inside lamellar sheets as an intermediate between LAM and CYL structures.

Concerning the supramolecules' systems mentioned above, they generally show an even more rich phase behavior if compared to conventional block copolymer systems [11–14,21,34]. For example, in some cases five different microphase morphologies have been observed as a function of temperature [34]. The main reason for such multi-phase behavior is the hydrogen bonding nature of the side chain attachment and the weakening of this bonding with temperature [11,22,35]. It has been also reported that an additional factor, which affects the behavior of PS-*b*-P4VP(PDP)$_x$ and PS-*b*-P4VP(MSA)$_y$(PDP)$_x$ systems, is the solubility of PDP in the PS phase at elevated temperatures [36]. In this respect, the complex of PI-*b*-P2VP with OG appears to be simpler than the above-mentioned systems with PDP, since PI remains apparently insoluble for OG in the whole temperature region investigated. Nevertheless, our previously published SAXS data showed that the phase behavior of the PI-*b*-P2VP(OG) system is full of surprises [22].

In this article, the LAM-to-CYL transition observed on heating the PI-*b*-P2VP(OG)$_{1.0}$ supramolecules' system both in quiescent conditions and under large amplitude oscillatory shear (LAOS) will be considered in detail. Based on the SAXS data obtained a novel mesostructure, referred to as deformed hexagonal structure (DHS), will be reported as a possible intermediate between the lamellar and cylindrical morphology.

2. Experimental

The supramolecules' system investigated consists of a complex of poly(1,4-isoprene)-*block*-poly(2-vinylpyridine) (PI-*b*-P2VP) and octyl gallate (OG), i.e., 4-octyl-3,4,5-trihydroxybenzoate, which interacts with the P2VP block via hydrogen bonding. The PI-*b*-P2VP block copolymer with polydispersity of 1.06 and molecular weights of the PI and P2VP blocks of 30,000 and 2800 g/mol, respectively, was obtained from Polymer Source and used as received. The expected ratio of isomers in the PI block is the following: 81 mol% of *cis*-1,4-addition, 15 mol% of *trans*-1,4-addition and 4 mol% of 3,4-addition. OG was obtained from Sigma–Aldrich and it was purified by recrystallizing from an ethanol/chloroform (9:1 volume ratio) azeotropic mixture prior to use.

The system PI-*b*-P2VP(OG)$_x$, with $x = 1.0$ denoting the ratio between the number of OG molecules and pyridine groups (Scheme 1), was prepared according to the procedure already described [22]. First, the PI-*b*-P2VP copolymer was dissolved in chloroform to a concentration less than 2% (w/w). Then the required amount of OG was added into the solution, and the system was allowed to form a complex for 24 h. After slow evaporation of the solvent in air, the samples were additionally dried in vacuum at 40 °C for 48 h.

SAXS measurements were performed at the European Synchrotron Radiation Facility (ESRF, beamline BM26 "DUBBLE") in Grenoble [37]. Experiments were carried out with the X-ray wavelength $\lambda = 0.124$ nm ($E = 10$ keV). The size of the primary beam at the sample position was ca. 0.2 × 0.2 mm. Scattering vector

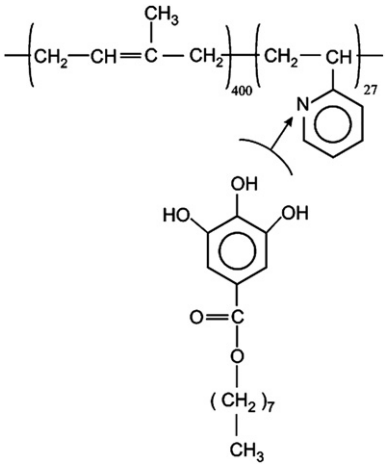

Scheme 1. Hydrogen-bonded complex of PI-*b*-P2VP and octyl gallate (OG).

magnitude was calculated as $q = (4\pi/\lambda)\sin\theta/2$, where θ is the scattering angle. The sample–detector distance was ca. 8 m.

Shearing of the samples was conducted using a home-made tooth rheometer, specially designed to perform in situ SAXS on samples subjected to large amplitude oscillatory shear (LAOS) [38,39]. This device is a kind of plate–plate rheometer, where instead of conventional relatively large-diameter plates, a couple of small size teeth are used in order to decrease both the amount of material investigated and the path of the primary X-ray beam in the sample. In this study, a tooth couple of 5 × 3 mm in size has been employed.

In situ SAXS experiments with the rheometer were performed on heating in the temperature range of 60–210 °C. The primary X-ray beam was directed into the rheometer gap along the shear vector direction (x-axis) and all in situ SAXS images were obtained as tangential patterns in the q_y–q_z scattering plane, as the most informative patterns for hexagonally assembled cylinders. A cartoon of the experimental set-up is shown elsewhere [39]. The rheometer was operated in a continuous oscillatory shear mode with a shear strain of ca. 100% and a frequency of 0.5 Hz. On heating the gap between the rheometer teeth slightly decreased, resulting in an increase (within 20%) in the shear strain. Rheological characteristics, such as the storage and loss moduli G' and G'', respectively, as well as the phase angle φ, were also measured during the in situ experiments. Since the sample was subjected to LAOS and therefore was not in the linear deformation mode, the measured parameters are not truly G' and G'' and they should be considered only as convenient quantities to follow an alignment experiment.

To avoid a temperature difference between SAXS measurements on shear and without shear, the latter were also performed using the oven of the tooth rheometer. In all experiments the heating rate was ca. 1.5 °C/min. The nitrogen was purged through the rheometer oven to prevent sample degradation. SAXS data were collected for 30 s per frame.

For transmission electron microscopy (TEM) ultra thin sections (approximately 70 nm) of PI-*b*-P2VP(OG)$_{1.0}$ samples were cryomicrotomed at $T = -100$ °C. Sections were picked up onto 600-mesh copper grids and, in order to enhance contrast, the microtomed sections were stained for 2–3 h in vapors of I_2 crystals, which selectively stains the P2VP domains. Bright-field TEM was performed on FEI Tecnai 12 transmission electron microscope operating at an accelerating voltage of 120 kV. To study the high temperature structure, the samples were first annealed at $T = 165$ °C and thereafter rapidly quenched to ca. $T = -180$ °C using liquid propane.

3. Results and discussion

3.1. SAXS measurements on non-sheared PI-b-P2VP(OG)$_{1.0}$

Azimuthally averaged SAXS patterns of the sample recorded on heating from 25 to 215 °C with a rate of 1.5 °C/min are presented in Fig. 1a. Such a low heating rate was used to allow the system to adopt a structure as close to equilibrium as possible. The data shown turned out to be very similar to those obtained with a faster heating rate of 10 °C/min [22]. At low temperatures a lamellar morphology is revealed and the periodicity of the structure equal to 30.6 nm at room temperature remains practically the same up to 125 °C. Above 195 °C the sample shows the characteristic pattern of hexagonally packed cylinders spaced at $a = 25.9$ nm from each other. In the intermediate temperature region extending from ca. 130 to 190 °C, a number of peculiar SAXS patterns are observed that do not correspond to any of the known intermediate morphologies, such as gyroid structure or hexagonally perforated layers. All our attempts to interpret those patterns as a simple coexistence of the lamellar and cylindrical morphologies that could be observed on the relatively fast heating (10 °C/min) were also not satisfactory [22]. Since in this study the heating of the PI-*b*-P2VP(OG)$_{1.0}$ sample was slow (ca. 1.5 °C/min) and the glass transition temperature (T_g) of the PI and P2VP(OG) domains was ca. −100 and 40 °C, respectively, the state of the sample at the intermediate temperatures, which are more than 100 °C above the T_g of the P2VP(OG) domains, is believed to be close to equilibrium. This suggests the existence of a mesophase in between the LAM and CYL structures, which was simply referred to as intermediate structure in our previous publication [22].

To obtain more detailed information on the morphological changes occurring with temperature, typical 2D SAXS patterns of the LAM, intermediate and CYL structures are presented in Fig. 2. Because of slight squeezing of the sample on loading in the rheometer, the lamellar pattern is somewhat anisotropic, showing three orders of meridional reflections with the position of the first order at $q^* = 0.205$ nm^{-1} (Fig. 2a). This pattern, practically not changing up to 125 °C, is a fingerprint for a moderate alignment of lamellar layers along the horizontal (x–y) plane. This alignment turned out to be very useful for further elucidation of the intermediate structure. Above 125 °C the main q^*-peak, as well as the higher order peaks, starts shifting to higher scattering angles, reaching $q^* = 0.235$ nm^{-1} at 155 °C (Fig. 3). We note here that this specific temperature of 125 °C does not correspond to the T_g of either the PI or P2VP(OG)$_{1.0}$ domains. As will be discussed further on, the observed behavior is most likely due to the specific nature of the supramolecular system.

As seen from Fig. 3a, apart from the shift of the originally lamellar peaks, four new peaks appear and altogether at 155 °C a series of peaks located at ca. 0.21, 0.24, 0.34, 0.40, 0.48 and 0.62 nm^{-1} are observed. Except for the two relatively weak peaks at $q = 0.21$ and 0.34 nm^{-1}, the others are spaced at a ratio of 1.0:1.70:2.02:2.64, which is quite close to the characteristic ratio of $1 : \sqrt{3} : \sqrt{4} : \sqrt{7}$ known for hexagonally packed cylindrical structure (CYL). However, the two above-mentioned weak peaks, each of which originates from four *off-meridional* reflections (see the 2D image in Fig. 2b)

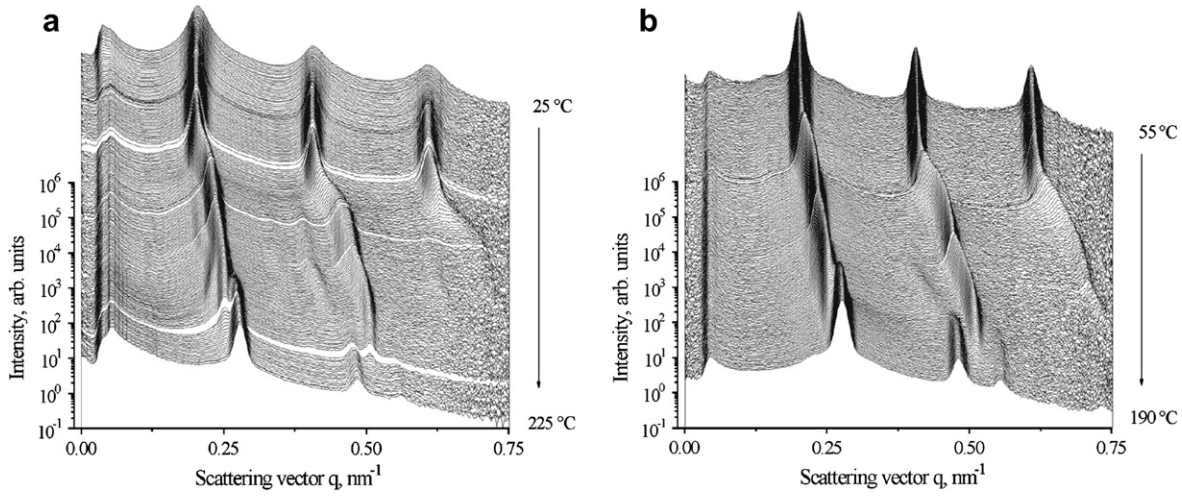

Fig. 1. Azimuthally averaged SAXS patterns obtained from PI-*b*-P2VP(OG)$_{1.0}$ on slow heating: (a) no shear; (b) on shear.

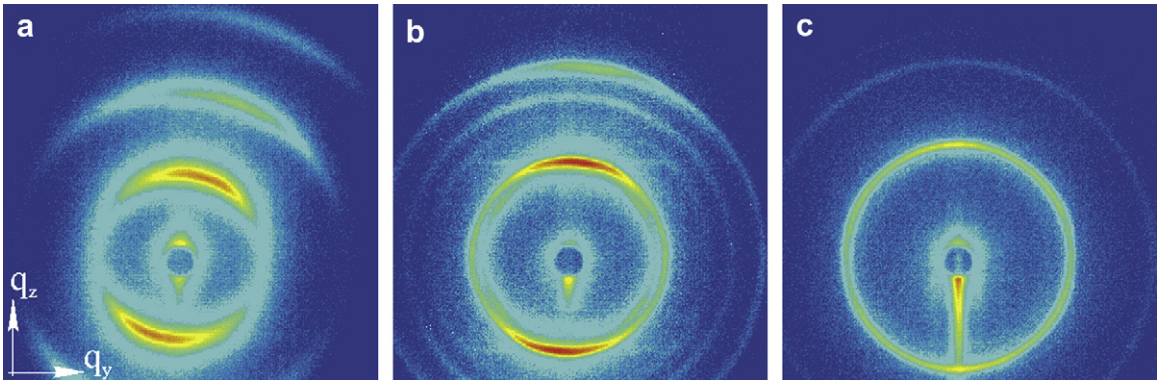

Fig. 2. SAXS images of PI-*b*-P2VP(OG)$_{1.0}$ obtained without any shear imposed: (a) lamellar (LAM) at 25 °C, (b) intermediate structure (DHS) at 155 °C, and (c) hexagonally packed cylindrical structure (CYL) at 210 °C.

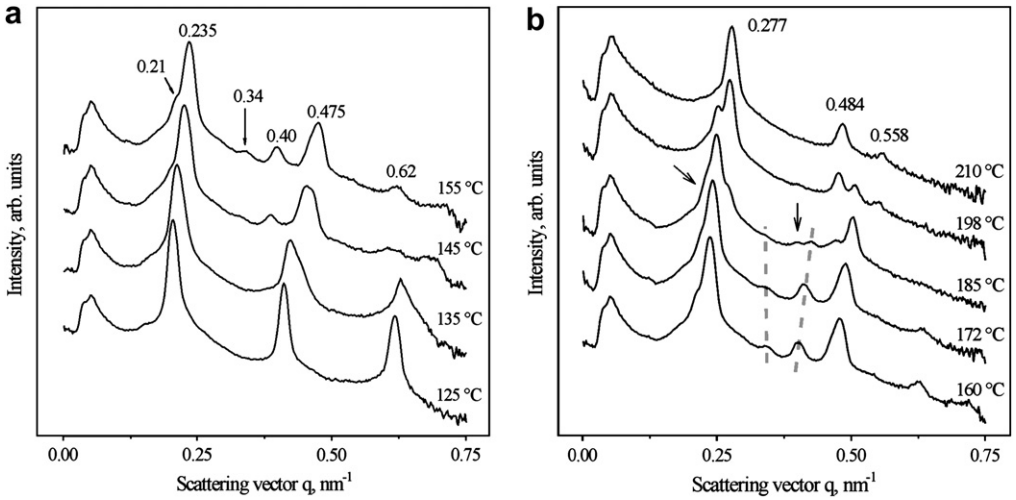

Fig. 3. Characteristic SAXS patterns obtained upon heating without shear: (a) LAM-to-DHS transition; (b) DHS-to-CYL transition.

indicate that the structure formed is more complex than just the CYL one. On the other hand, the pattern observed neither corresponds to the gyroid nor hexagonally perforated layer structures.

Based on the 2D image of Fig. 2b, a deformed hexagonal structure (DHS) is suggested as a model of the sample structure observed at the intermediate temperatures. A cartoon of the DHS is presented in Fig. 4a, showing an array of ellipsoidal cylinders ordered in an oblique lattice with $a = 35.6$ nm, $b = 31.8$ nm and $\gamma = 124^\circ$ (see Fig. 4b). The specific feature of this DHS is the following ratio between a and b: $a = 2b\cos(180^\circ - \gamma)$. The main diffraction planes (hk) of the oblique lattice are shown in Fig. 4b, while the calculated interplanar distances d_{hk} are collected in Table 1 to compare them with the experimental data (d_{exp}). In general good agreement between the calculated and experimental values is observed. As also seen from Table 1, the number of DHS reflections considerably exceeds that ascribed to a CYL structure. According to the DHS model, the ellipsoidal cylinders adopt the initial orientation of the lamellar layers (Fig. 4a), suggesting an epitaxial growth mechanism [30]. Consequently, the most prominent scattering corresponding to the (01) reflections is still located on the meridian (Fig. 2b), similar to the anisotropic pattern of the lamellar structure observed at lower temperatures (Fig. 2a). On the other hand, the four off-meridional reflections at $q = 0.21$ nm^{-1} are due to the (10) and ($\bar{1}1$) diffraction planes with $d_{hk} = 29.5$ nm, which are tilted with respect to the horizontal (01) plane by $\pm\gamma = 124^\circ$. The off-meridional reflections are supposed to be visible only when the cylinders are oriented in the direction close to the direction of the primary X-ray beam. In the non-sheared sample the number of those cylinders is expected to be quite small, explaining the relatively weak intensity of these reflections compared to the meridional (01) ones.

Table 1
Comparison of the proposed DHS model with the experimental data

CYL	DHS (oblique)				
$h^2 + k^2 + hk$	h	k	d_{hk}	d_{exp}	q_{exp}
1	1	0	29.50	29.9 (w)	0.21
	−1	1			
	0	1	26.38	26.7 (vs)	0.235
3	2	−1	17.79	18.5 (w)	0.34
	1	1	15.77	15.7 (s)	0.40
	−1	2			
4	2	0	14.75	–	–
	−2	2			
	0	2	13.19	13.2 (s)	0.475
7	3	−1	11.57	11.6 (vw)	0.54
	3	−2			
	2	1	10.60	10.13 (w)	0.62
	−2	3			
	1	2	10.12		
	−1	3			
9	3	0	9.83		
	−3	3			
	0	3	8.79		

vs – very strong, s – strong, w – weak, vw – very weak.

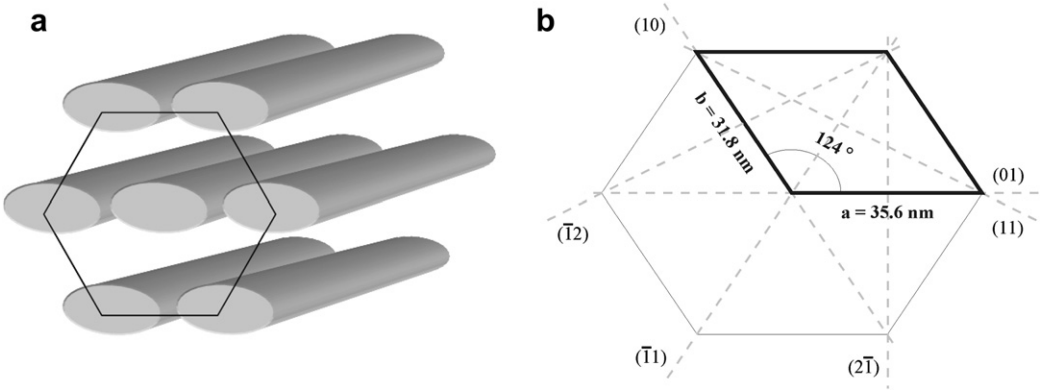

Fig. 4. (a) Model of the DHS with ellipsoidal cylinders packed in an oblique lattice. (b) Proposed oblique unit cell with $a = 2b\cos(180^\circ - \gamma)$, where $b = 31.8$ nm and $\gamma = 124^\circ$ to correspond the DHS pattern at 155 °C (see Fig. 2b); the main diffraction planes are indicated with dash lines.

According to the model, the $(2\bar{1})$ diffraction planes should produce two equatorial reflections at $q = 0.349\ \mathrm{nm}^{-1}$, corresponding to $d_{hk} = 17.8$ nm (see Table 1). Though the calculated distance is close to $d_{exp} = 18.5$ nm, no prominent intensity maximum is in fact found on the equator, instead four off-meridional arches at $q_{exp} = 0.34\ \mathrm{nm}^{-1}$ are observed (see Fig. 2b). This discrepancy is most probably due to both the disorientation of cylinders with respect to the primary beam and the specific ellipsoidal character of the cylinders. Some imperfection in the DHS ordering may also affect the image. On the other hand, all other calculated data are in good agreement with the experimentally observed reflections (see Table 1). This suggests that the DHS introduced is an adequate model for the intermediated structure of the PI-*b*-P2VP(OG)$_{1.0}$ sample.

Due to the very low T_g of the PI domains and a quite low T_g of the P2VP(OG)$_{1.0}$ domains, as well as the fact that the DHS is stable only at temperatures above 130 °C, our attempts to get direct evidence of the ellipsoidal cylinders by TEM were not very successful. A typical image of the sample quenched from 165 °C into liquid propane is shown in Fig. 5. The main feature of the image is the presence of a lamellar morphology with very thin P2VP(OG)$_{1.0}$ layers (dark) surrounded by relatively thick PI layers (light). Since the weight fraction of PI in the sample is 74.4% such thin P2VP(OG)$_{1.0}$ layers could be in principle anticipated. However, the existence of the lamellar morphology itself, rather than a cylindrical one that is more expected at this percentage of PI, is believed to be due to the comb–coil architecture of the supramolecules, as will be discussed below. A close look at the TEM image reveals that the dark layers have relatively regular fluctuations in thickness (guided by solid lines), suggesting that the proposed ellipsoidal cylinders of DHS are indeed formed in the intermediated temperature region.

As seen from Fig. 3b, the DHS is stable up to ca. 185 °C where the first sign of the final cylindrical structure appears. Above 160 °C the DHS undergoes an additional transformation before completely vanishing. As indicated by dashed lines, while most of the DHS peaks shift towards higher scattering angles upon heating, the peak at $0.34\ \mathrm{nm}^{-1}$ is found to shift to slightly lower q-values. As discussed below, the gradual transformation of the ellipsoidal cylinders into more circular-shaped cylinders might result in the SAXS changes observed. At a temperature of 185 °C the q^* and $\sqrt{3}q^*$ peaks of the CYL structure become visible. Apart from these, two additional weak peaks indicated by arrows in Fig. 3b are observed at $q = 0.23$ and $0.40\ \mathrm{nm}^{-1}$. The nature of these peaks is not very clear yet, but since they are spaced at a ratio close to $1 : \sqrt{3}$ they might originate from some fluctuations in the DHS lattice parameters. Nevertheless, these two peaks, together with all other peaks of the DHS, gradually disappear on further heating, while the CYL structure characterized by a series of three peaks at ca. $q^* = 0.27\ \mathrm{nm}^{-1}$, $\sqrt{3}q^*$ and $2q^*$, is the only structure above 205 °C. A 2D image of the structure obtained at 210 °C is shown in Fig. 2c.

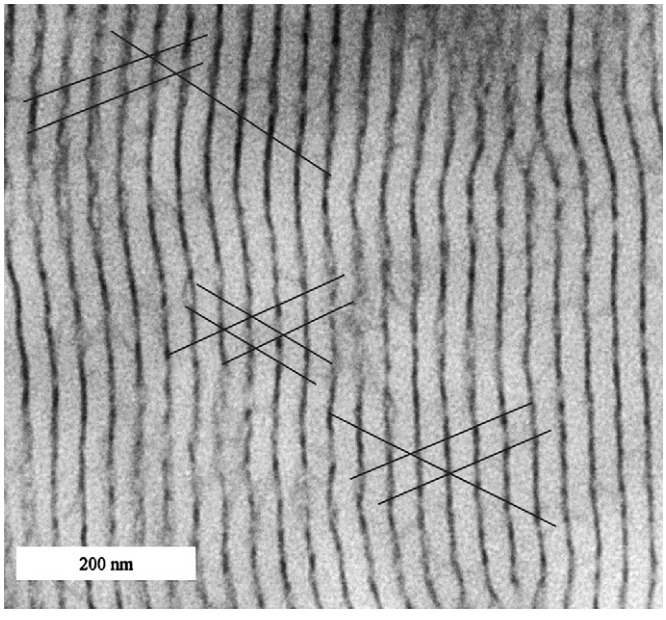

Fig. 5. TEM micrograph of PI-*b*-P2VP(OG)$_{1.0}$ quenched from 165 °C. P2VP(OG)$_{1.0}$ domains are dark in the image due to I_2 staining. Solid lines indicate regular fluctuations in thickness.

3.2. Discussion of the LAM–DHS–CYL transition

The main reason for the unique phase behavior of the PI-*b*-P2VP(OG)$_{1.0}$ system, i.e., firstly the constant lamellar structure spacing at low temperatures and secondly the formation of ellipsoidal cylinders packed into a DHS, must originate from the specific comb-copolymer nature of the system, where OG side chains are H-bonded to the P2VP block. It is generally known that an important aspect of microphase separation in the case of linear diblock copolymers is the tendency of the system to minimize the interface area. Another aspect is the fact that normally an OOT between different structures, e.g., lamellar-to-cylindrical transition may be induced by temperature only if the system is in the weak to intermediate segregation regime. In contrast to pure linear diblock copolymers, where the conformation of the polymer chains is dependent only on temperature, in the case of the PI-*b*-P2VP(OG)$_{1.0}$ supramolecular system the conformation of the P2VP blocks and the overall phase behavior are additionally strongly influenced by the presence of the H-bonded OG side chains. Like covalently bonded side chains, H-bonded side chains also occupy considerable space around the polymer backbone, forcing the P2VP blocks to adopt more stretched conformations. Especially if the side chains are present near the interface between PI and P2VP(OG) blocks, this may result in a tendency to create an outward curved interface of the P2VP(OG) domains. The fact that in the temperature region below 125 °C the lamellar structure is found to be the most stable state while the weight fraction of the P2VP(OG)$_{1.0}$ domain is only 25.6%, which is a clear manifestation of this side chain effect. Hence, the graft-like nature of the P2VP(OG)$_{1.0}$ block is essential for the specific phase behavior of PI-*b*-P2VP(OG)$_{1.0}$. In addition, another important aspect is the dynamic equilibrium nature of H-bonding, which depends both on temperature and the concentration of side chains. FTIR data showed [22] that a considerable reduction in the number of hydrogen-bonded pyridine groups is taking place only at temperatures above 100 °C. Therefore, the constant lamellar *d*-spacing up to 125 °C may be explained in terms of the stability of the H-bonds and, hence, of preserving the number of OG molecules attached to pyridine groups below this temperature. Reducing the number of side chains on further heating allows the P2VP blocks to adopt a more coil-like conformation, destabilizing the lamellar structure and inducing the transformation into a cylindrical structure. Since the weakening of the H-bonding proceeds gradually with temperature, there is still a considerable number of OG amphiphiles attached to the P2VP block at intermediated temperatures, keeping the backbone molecules in a slightly stretched conformation. For this reason the P2VP(OG)$_{1.0}$ domains are not perfectly circular cylinders but rather adopt a ellipsoidal cross-section. Due to this shape, the "cylinders" apparently prefer ordering into the DHS (Fig. 4a). In the literature a similar kind of deformed hexagonal packing was first reported for cylindrical micelles formed by low molecular weight surfactant molecules in water [40–42]. For polymer-based systems such a structure was observed for, e.g., aqueous polyelectrolyte–surfactant complexes, for which a distorted hexagonal structure with $a = b$ and $\gamma > 120°$ was suggested [43,44]. Another example is the SAXS study of a coil–

comb-like block copolymer [45], the morphology of which was also discussed in terms of a deformation of hexagonally structure. According to the literature, in all these cases, the driving force to induce some deformations in a regular cylindrical structure is the deviation of the interface curvature from the circular shape. In the surfactant complexes this deviation was induced by changing the head-to-tail ratio, while in the polymer systems the introduction of grafted side chains bonded either covalently [45] or ionically [43,44] results in similar structure deformation.

As already mentioned above, the strength of H-bonding is strongly dependent on temperature, causing the remarkable lability in the sample morphology. On further heating, the effective number of bonded OG molecules is considerably reduced, permitting the P2VP chains to become significantly less stretched. Because of this, the P2VP$(OG)_{1.0}$ domains forming the ellipsoidal "cylinders" of the DHS at intermediate temperatures transform to the more favorable circular cylinders of a regular CYL structure at high temperatures.

Apart from the influence of temperature, the level of hydrogen bonding in PI-*b*-P2VP$(OG)_x$ systems, and therefore their morphology, is known to be affected by shear [46]. To elucidate the influence of shear on the LAM-to-CYL transition in this particular PI-*b*-P2VP$(OG)_{1.0}$ system, additional in situ SAXS experiments were conducted. The results of these experiments are described below.

3.3. *In situ SAXS measurements of PI-b-P2VP$(OG)_{1.0}$ under LAOS*

Using the tooth rheometer [37,38], the supramolecules' system was subjected to LAOS with a strain amplitude of 100% and a frequency of 0.5 Hz. Azimuthally averaged SAXS patterns of the sample obtained on heating from 55 to 195 °C are shown in Fig. 1b, while changes in the phase angle φ and the storage G' and loss G'' moduli measured during these in situ SAXS experiment are presented in Fig. 6. Just after loading into the rheometer the sample shows relatively good alignment of lamellae parallel to the x–y plane (the shear plane). Three orders of lamellar reflections with the first order at $q^* = 0.21\ \mathrm{nm}^{-1}$ are observed on the meridian (Fig. 7a). Due to more significant squeezing of the sample, this pattern is even more anisotropic than that in Fig. 2a for the non-sheared sample.

When shear starts, the lamellar reflections become sharper and more intense, signaling an improvement in the lamellar structure alignment. Simultaneously, a decrease in the dynamic moduli G' and G'' as well as an increase in the phase angle φ is observed (Fig. 6). The SAXS image recorded at 80 °C is shown in Fig. 7b. Note that this SAXS pattern, as many other images obtained on shear and without shear, contains two specific "artifacts": (a) two weak meridional reflections just above the high intensity q^*-reflections and (b) horizontal stripes arising from both q^*- and $2q^*$-reflection. The origin of these "artifacts" is not clear yet. Most probably these features are an indication for some imperfection in the lamellar morphology. Another possible reason is the detector saturation occurring at a very high local rate of photons. In any case, these "artifacts" are most evident when the sample is of a lamellar structure and they gradually disappear with temperature when a LAM-to-CYL transition occurs. As seen from Fig. 6, at ca. 80 °C the phase angle φ reaches its largest value of 85°. On further heating a decrease is observed, resulting in ca. $\varphi = 75°$ at 130 °C. Such a decrease might indicate the development of in-plane modulations of the lamellar layers [30]. Another reason is the formation of relatively narrow and long lamellar domains, as the first step to a cylindrical structure, which is somewhat misaligned with respect to both the shear plane and the shear direction. The latter scenario is apparently corroborated by SAXS. The lamellar image recorded at 80 °C shows arc-like reflections exhibiting considerable azimuthal spreading, especially for higher order peaks (Fig. 7b). At ca. 130 °C the arches transform eventually into complete rings that are still anisotropic, exhibiting much higher intensity on the meridian. Similar to the non-sheared sample, the lamellar periodicity in the sheared sample is ca. 30.0 nm from low temperatures up to 125 °C.

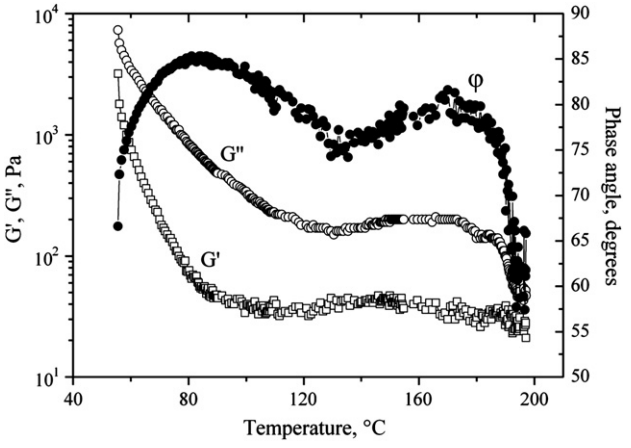

Fig. 6. Temperature dependence of the dynamic moduli G' and G'' and the phase angle φ obtained for the PI-*b*-P2VP$(OG)_{1.0}$ sample during in situ SAXS measurements.

On further heating, the sheared sample exhibits considerable changes in SAXS patterns. These changes become most visible at 155 °C (Figs. 7d and 8a), when apart from the original lamellar peaks shifted towards higher scattering angles, a new peak arises at $q = 0.40\ \mathrm{nm}^{-1}$. With respect to the main q^*-peak at $0.234\ \mathrm{nm}^{-1}$, the first three peaks observed are spaced at a ratio of 1:1.69:2.02, which is quite close to the characteristic ratio of a regular CYL structure (Fig. 8a). For comparison, the SAXS pattern of the non-sheared sample obtained at 155 °C is also presented in Fig. 8a. The main difference between these patterns is the presence of two weak peaks marked by arrows in the case of the non-sheared sample, the structure of which was referred as to DHS. Therefore, for the sheared sample, the absence of such peaks suggests that its structure is much closer to a regular CYL structure than the DHS formed by ellipsoidal cylinders. However, a close inspection of the 2D images of Fig. 7d–f reveals that at 155 °C the sheared sample has still a DHS-like morphology. Similar to the non-sheared sample, four rather faint off-meridian reflections located on the inner side of the q^*-scattering ring are observed for the sheared sample at 155 °C (Fig. 7d). These reflections that are not noticeable in the 1D pattern of Fig. 8a, are evidence of some distortions in the regular hexagonal order of P2VP(OG) cylinders. The presence of four weak off-meridian reflections located at ca. $\sqrt{3}q^*$ is also an indication of the imperfect hexagonal order and low alignment of the cylinders along the shear flow (x-axis), coinciding with the primary X-ray beam direction.

All this indicates that the structure of the sheared sample at 155 °C is also of the DHS type, however, in this case the deformation of hexagonal order is not as large as it was for the non-sheared sample. Interestingly, after cessation of shear the image of Fig. 7d becomes similar to that shown in Fig. 2b, showing a clear influence of shear on the sample morphology.

As explained above for the non-sheared sample, the main reason for appearance of the ellipsoidal cylinders is the strongly stretched conformation of the P2VP chains that results from the H-bonding with OG side chains. On the other hand, our previous experimental data suggest that shear may facilitate the temperature-induced breaking of H-bonds [46]. This results in a much faster transformation of the ellipsoidal cylinders into regular circular ones upon shear, since being less bonded with OG the P2VP blocks can readily adopt a more coil-like conformation. Indeed, at 185 °C new arc reflections start to appear (Fig. 7e) and they become clearly visible at 190 °C as peaks spaced at a ratio of $1 : \sqrt{3} : \sqrt{4}$ (Fig. 7f).

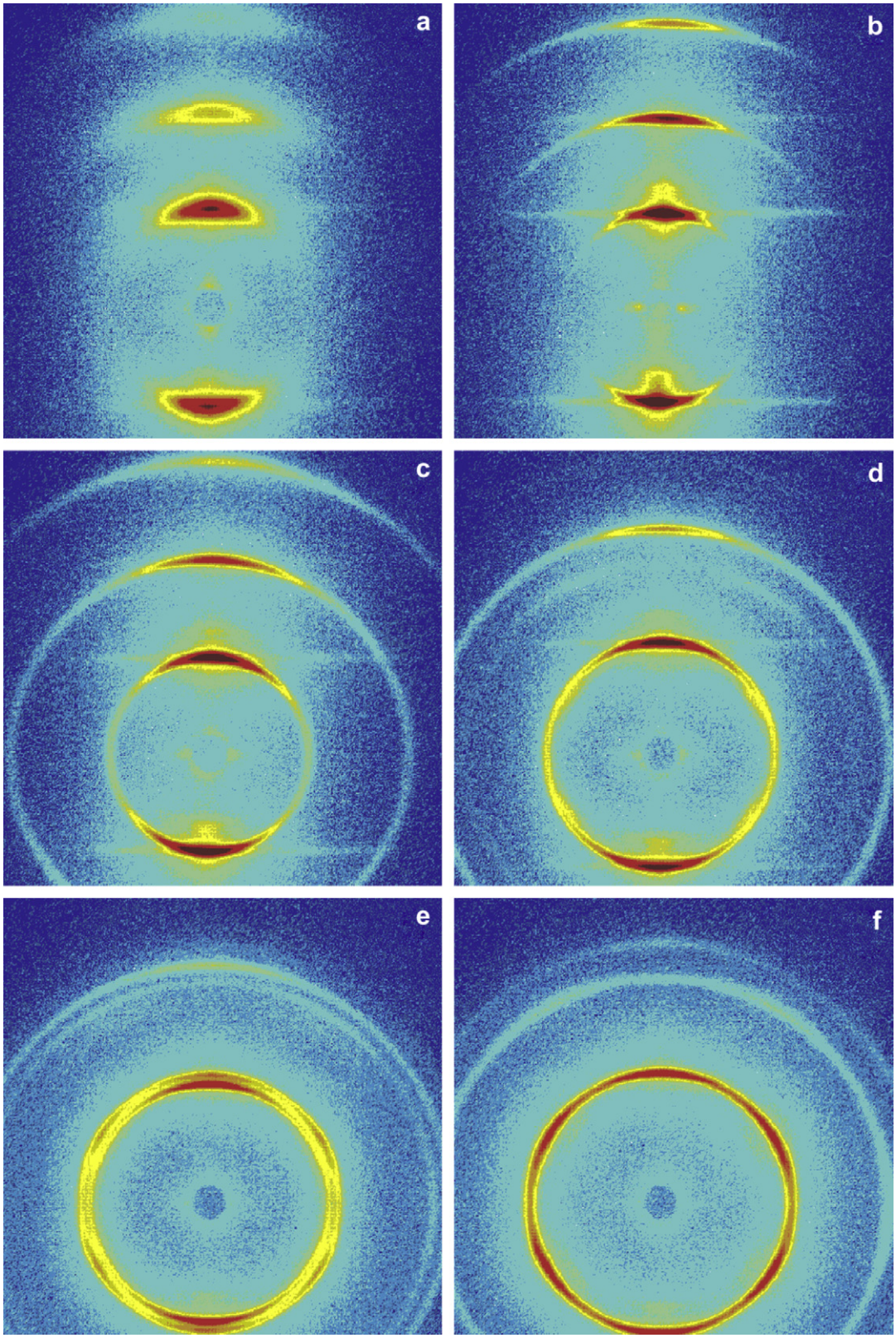

Fig. 7. Characteristic SAXS images of the PI-*b*-P2VP(OG)$_{1.0}$ sample obtained: (a) at rest – just after loading into the rheometer at 55 °C and on oscillatory shear with a stain amplitude of 100% and a frequency of 0.5 Hz at (b) 80, (c)130, (d) 155, (e) 185 and (f) 190 °C.

Meanwhile the initial DHS peaks are gradually vanishing, disappearing completely at 195 °C which is 10 °C lower than the corresponding temperature found for the non-sheared sample. Fig. 8b compares the patterns observed from the sheared and non-sheared samples at 195 °C. For the latter, the additional peaks originating from the DHS are marked with arrows.

Interestingly, the formation of the DHS-like structure is also manifested by rheology (Fig. 6). The phase angle φ gradually

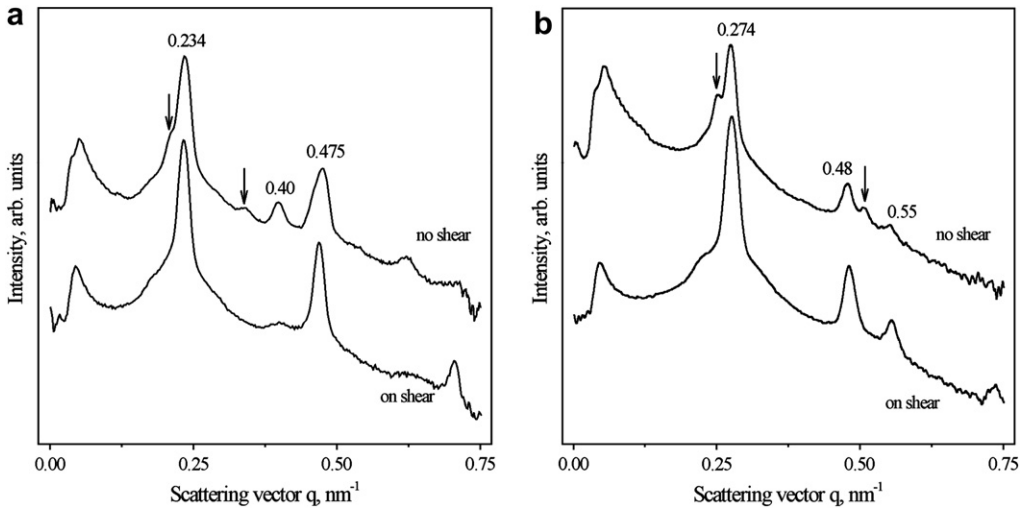

Fig. 8. Comparison of the SAXS patterns of PI-*b*-P2VP(OG)1.0 recorded both with and without shear at (a) 155 and (b) 195 °C.

increases in the temperature range of 130–170 °C, reaching its maximum value of ca. 80°. This corresponds to the formation of DHS-like cylinders that become more and more aligned along the shear flow. However, at temperatures from 170 to 190 °C, the phase angle shows a second decay, indicating new structural changes in the sample, i.e., the DHS–CYL transition.

Similar to a slightly different PI-*b*-P2VP(OG)0.75 system [46], the DHS–CYL transformation observed for the PI-*b*-P2VP$(OG)_{1.0}$ sample can be referred to as a cylinder-to-cylinder transition, characterized by an abrupt change in the diameter of the P2VP$(OG)_{1.0}$ cylinders, caused by practically complete breaking of the hydrogen bonding. Because of such diameter collapse, the packing of P2VP(OG)1.0 cylinders becomes more dense, resulting in a phase angle decrease. In fact, the decrease shown in Fig. 6 is much larger than it was found for the system with a lower amount of OG [46]. This is presumably due to the fact that in the case of PI-*b*-P2VP$(OG)_{1.0}$ the transition occurs at even higher temperatures, where both the local disordering and the disorientation of cylindrical domains on shear become quite possible.

It is important to note that not only because of the position of the reflections in Fig. 7d and e but also due to the fact that these images were obtained on shear, any interpretation of the sample morphology in terms of a 3D structure, like gyroid or HPL, is hardly possible. Besides, we would like to mention that despite the high temperatures used, the samples investigated remained transparent and soluble, indicating that no significant cross-linking took place. Therefore, all changes observed by SAXS are considered as morphological transitions proceeding without noticeable influence of chemical reactions.

4. Concluding remarks

The comb-shaped architecture of the PI-*b*-P2VP$(OG)_{1.0}$ supramolecules leads to a very peculiar phase behavior of the system, showing the formation of a deformed hexagonal structure (DHS) as an intermediate between the low temperature LAM and high temperature CYL structures. Due to H-bonding of OG with P2VP, the latter is in a strongly stretched conformation. This gives rise to a LAM structure at low temperatures even though the weight fraction of the PVP(OG) comb-like domain is only 25.6%. The periodicity of the structure remains remarkably constant on heating the sample up to 120 °C, which was also explained in terms of H-bonding being quite stable at such low temperatures. Due to H-bond breaking occurring at higher temperatures, the effective number of OG side chains attached to the P2VP backbone is reduced, resulting in a more coil-like conformation of P2VP. In turn, the latter induces a LAM–DHS–CYL transition. At high temperatures, i.e., at above 210 °C for the non-sheared sample, when almost complete breaking of H-bonds occurs, a CYL structure is the only structure of the PI-*b*-P2VP$(OG)_{1.0}$ system. At intermediate temperatures, a considerable number of OG side chains are still attached to the P2VP block. Because of this, the P2VP chains remain considerably stretched and, as a consequence, the LAM morphology transforms first into a deformed hexagonal structure (DHS) with "cylinders" having an ellipsoidal cross-section, rather than directly into a regular hexagonally ordered cylindrical structure. An oblique unit cell with $a = 35.6$ nm, $b = 31.8$ nm and $\gamma = 124°$ is proposed for this intermediate DHS at 155 °C.

The sample subjected to LAOS shows a similar morphological behavior with temperature if compared with the non-sheared one. However, the DHS of the sheared sample is much closer to a regular hexagonally packed cylindrical structure and it vanishes at a temperature that is ca. 10 °C lower than the corresponding transition temperature of the non-sheared sample. This behavior is explained in terms of the facilitation of H-bond breaking by shear.

The phase behavior of the sample observed on shear by SAXS is in agreement with the rheological measurements. In particular, both upon the LAM-to-DHS and DHS-to-CYL transitions, a decrease in the phase angle φ was recorded which was quite significant in the latter case. This finding is explained by the formation of a more densely packed cylindrical structure. However, the possibility of some local disordering and disorientation of CYL domains in the sheared sample at such high temperatures should not be excluded.

Finally, it should be noted that due to the very low T_g of the PI block and the quite low T_g of the P2VP$(OG)_{1.0}$ block, the TEM image obtained after quenching of PI-*b*-P2VP$(OG)_{1.0}$ from 165 °C reveals mostly a lamellar structure, although some signs of the DHS proposed were also visible.

Acknowledgement

Beam time on the DUBBLE beamline of ESRF (Grenoble, France) has kindly been made available by The Netherlands Organization for Scientific Research (NWO). We are grateful to Wim Bras and Florian Meneau for experimental assistance and helpful discussion.

References

[1] Hamley IW. The physics of block copolymers. Oxford: Oxford University Press; 1998.

[2] Fredrickson GH, Bates FS. Phys Today 1999;52:32.
[3] Muthukumar M, Ober CK, Thomas EL. Science 1999;277:1225.
[4] Fasolka MJ, Mayes AM. Annu Rev Mater Res 2001;31:323.
[5] Förster S, Plantenberg T. Angew Chem Int Ed 2002;41:688.
[6] Hamley IW. Angew Chem Int Ed 2003;42:1692.
[7] Liu T, Burger C, Chu B. Prog Polym Sci 2003;28:5.
[8] Park C, Yoon J, Thomas EL. Polymer 2003;44:6725.
[9] Abetz V, Simon PFW. Adv Polym Sci 2005;189:125.
[10] Hillmyer MA. Adv Polym Sci 2005;190:137.
[11] Ruokolainen J, Mäkinen R, Torkkeli M, Serimaa R, ten Brinke G, Ikkala O. Science 1998;280:557–60.
[12] Ikkala O, ten Brinke G. Science 2002;295:2407–9.
[13] Ikkala O, ten Brinke G. Chem Commun 2004:2131–7.
[14] ten Brinke G, Ruokolainen J, Ikkala O. Adv Polym Sci 2007;207:113–77.
[15] Mäkinen R, de Moel K, de Odorico W, Ruokolainen J, Stamm M, ten Brinke G, et al. Adv Mater 2001;13:117–21.
[16] Fahmi AW, Braun H-G, Stamm M. Adv Mater 2003;15:1201–4.
[17] Sidorenko A, Tokarev I, Minko S, Stamm M. J Am Chem Soc 2003;125:12211–6.
[18] Fahmi AW, Stamm M. Langmuir 2005;21:1062–6.
[19] de Moel K, van Ekenstein G, Nijland H, Polushkin E, ten Brinke G, Maki-Ontto R, et al. Chem Mater 2001;13:4580–3.
[20] Fahmi AW, Brüning H, Weidisch R, Stamm M. Macromol Mater Eng 2005;290:136.
[21] van Zoelen W, Alberda G, Polushkin E, Ikkala O, ten Brinke G. Soft Matter 2005;1:280–3.
[22] Bondzic S, de Wit J, Polushkin E, Schouten AJ, ten Brinke G, Ruokolainen J, et al. Macromolecules 2004;37:9517.
[23] Sakurai S, Kawada H, Hashimoto T, Fetters LJ. Macromolecules 1993;26:5796.
[24] Kim JK, Lee HH, Ree M, Lee KB, Park Y. Macromol Chem Phys 1998;199:641.
[25] Ryu CY, Vigild ME, Lodge TP. Phys Rev Lett 1998;81:5354.
[26] Krishnamoorti R, Modi MA, Tse MF, Wang HC. Macromolecules 2000;33:3810.
[27] Vigild ME, Almdal K, Mortensen K, Hamley IW, Fairclough JPA, Ryan AJ. Macromolecules 1998;31:5702.
[28] Floudas G, Ulrich R, Wiesner U, Chu B. Europhys Lett 2000;50:182.
[29] Wang CY, Lodge TP. Macromolecules 2002;35:6997.
[30] Hamley IW, Koppi KA, Rosedale JH, Bates FS, Almdal K, Mortensen K. Macromolecules 1993;26:5959.
[31] Ryu JH, Oh NK, Zin WC, Lee M. J Am Chem Soc 2004;126:3551.
[32] Hajduk DA, Gruner SM, Rangarajan P, Register RA, Fetters LJ, Honeker C, et al. Macromolecules 1994;27:490.
[33] Jeong U, Lee HH, Yang LH, Kim JK, Okamoto S, Aida S, et al. Macromolecules 2003;36:1685.
[34] Valkama S, Ruotsolainen T, Nykanen A, Laiho A, Kosonen H, ten Brinke G, et al. Macromolecules 2006;39:9327.
[35] Eichhorn K-J, Fahmi AW, Adam G, Stamm M. J Mol Struct 2003;161:661–2.
[36] van Zoelen W, Alberda G, Ikkala O, ten Brinke G. Macromolecules 2006;39:6574–9.
[37] Bras W, Dolbnya IP, Detollenaere D, van Tol R, Malfois M, Greaves GN, et al. J Appl Crystallogr 2003;36:791–4.
[38] Polushkin E, van Ekenstein G, Dolbnya I, Bras W, Ikkala O, ten Brinke G. Macromolecules 2003;36:1421.
[39] Polushkin E, van Ekenstein G, Ikkala O, ten Brinke G. Rheol Acta 2004;43:364.
[40] Luzzati V, Mustacchi H, Skoulios A, Husson F. Acta Crystallogr 1960;13:660.
[41] Kekicheff P, Cabane B. J Phys I 1987;48:1571.
[42] Auvray X, Petipas C, Anthore R, Rico I, Lattes A. J Phys Chem 1989;93:7458.
[43] Zhou SQ, Hu HB, Burger C, Chu B. Macromolecules 2001;34:1772.
[44] Zhou SQ, Burger C, Chu B. J Phys Chem B 2004;108:10819.
[45] Burger C, Micha MA, Oestreich S, Forster S, Antonietti M. Europhys Lett 1998;42:425.
[46] Polushkin E, Bondzic S, de Wit J, van Ekenstein G, Dolbnya I, Bras W, et al. Macromolecules 2005;38:1804.